Conformational Propensities of Protein Folding Intermediates: Distribution of Species in the 1S, 2S, and 3S Ensembles of the [C40A,C95A] Mutant of Bovine Pancreatic Ribonuclease A[†]

William J. Wedemeyer, Xiaobing Xu, Ervin Welker, and Harold A. Scheraga*

Baker Laboratory of Chemistry and Chemical Biology, Cornell University, Ithaca, New York 14853-1301

Received October 5, 2001; Revised Manuscript Received December 4, 2001

ABSTRACT: A key problem in experimental protein folding is that of characterizing the conformational ensemble of denatured proteins under folding conditions. We address this problem by studying the conformational propensities of reductively unfolded RNase A under folding conditions, since earlier work has indicated that the *equilibrium* conformational ensemble of fully reduced RNase A resembles the *transient* conformational ensemble of a burst-phase folding intermediate of disulfide-intact RNase A. To assess these propensities, the relative disulfide-bond populations of the 1S, 2S, and 3S ensembles of the [C40A,C95A] mutant of RNase A were measured. Thirteen of the fifteen possible disulfide bonds are observed, consistent with earlier results and with the rapid reshuffling and lack of stable tertiary structure in these ensembles. This broad distribution contradicts recent observations by another group, but rigorous cross-checks show unambiguously that our data are self-consistent whereas their data are not. The distributions of disulfide bonds in the wild-type and mutant proteins show a power-law dependence on loop length, with an exponent that is significantly smaller than the exponents of either ideal or excluded-volume polymers. The 65−72 disulfide bond is much more strongly favored than would be predicted by this power law, consistent with earlier peptide studies and the disulfide-bond distributions of the 1S and 2S ensembles in wild-type RNase A. Experimental evidence suggests that this preference results from conformational biases in the backbone, rather than from differing accessibilities or reactivities of the two cysteine residues. In general, the other disulfide species do not deviate significantly from the power-law dependence, indicating that the conformational biases are relatively weak.

A key problem in experimental protein folding is that of characterizing the conformational ensemble of denatured proteins under folding conditions (*1*), such as that which occurs in the burst phase of stopped-flow folding experiments (*2*, *3*). The chief experimental difficulty is that such ensembles are by nature transient (since the proteins continue to fold), and their short-lived existence does not allow normal atomic-resolution structural techniques to be applied. The great heterogeneity of such ensembles also makes it difficult to characterize them structurally. However, the characterization of this conformational ensemble is critical to understanding the mechanism of protein folding.

We address this problem here by studying the conformational propensities of reductively unfolded RNase A[1] under folding conditions, since earlier work has indicated that the *equilibrium* conformational ensemble of fully reduced RNase A resembles the *transient* conformational ensemble of a burst-phase folding intermediate of disulfide-intact RNase A (*4*−*6*). To assess these propensities, the relative disulfide-bond populations of the 1S, 2S, and 3S ensembles of the [C40A,C95A] mutant of RNase A were measured, as in earlier experiments in which the 1S and 2S disulfide-bond distributions of wild-type RNase A were measured (*7*, *8*). This mutant has only three disulfide bonds, which simplifies the analysis and even allows the relative percentages of disulfide species in the 3S ensemble to be determined from the relative percentages of its disulfide bonds (see the Results). This mutant is also attractive because it is an analogue of the structured intermediate des[40−95], which appears on the major oxidative folding pathway for wild-type RNase A (*6*).

Wild-type RNase A has four disulfide bonds in its native state (Cys26−Cys84, Cys40−Cys95, Cys58−Cys110, and Cys65−Cys72) (Figure 1; *9*−*14*) and spontaneously regener-

[†] This work was supported by the National Institute of General Medical Sciences of the National Institutes of Health (Grant GM-24893). Support was also received from the National Foundation for Cancer Research. W.J.W. is an NIH Postdoctoral Fellow (1998−2001). X.X. is a Leukemia Society of America Special Fellow (1995−1997).

* To whom correspondence should be addressed. Telephone: (607) 255-4034. Fax: (607) 254-4700. E-mail: has5@cornell.edu.

[1] Abbreviations: RNase A, bovine pancreatic ribonuclease A; des-[40−95], three-disulfide intermediate of ribonuclease A containing three native disulfide bonds, but lacking the disulfide bond between Cys40 and Cys95; [C40A,C95A], mutant analogue of des[40−95] obtained by substituting alanines for Cys40 and Cys95 using site-directed mutagenesis; [C65A,C72A] and [C65S,C72S], similar mutants of des-[65−72]; R, completely reduced species; 1S, one-disulfide intermediates; 2S, two-disulfide intermediates; 3S, three-disulfide intermediates; N, folded [C40A,C95A]; AEMTS, (2-aminoethyl)methanethiosulfonate [$(NH_2)C_2H_4SSO_2CH_3$]; NTSB, disodium 2-nitro-5-thiosulfobenzoate; DTT^{red}, reduced dithiothreitol; DTT^{ox}, oxidized dithiothreitol; EDTA, ethylenediaminetetraacetic acid; Tris, tris(hydroxymethyl)aminomethane; MS, mass spectrometry; MALDI-TOF, matrix-assisted laser desorption ionization time-of-flight; HPLC, high-performance liquid chromatography; DDS, disulfide-detection system.

10.1021/bi011893q CCC: $22.00
Published on Web 01/09/2002

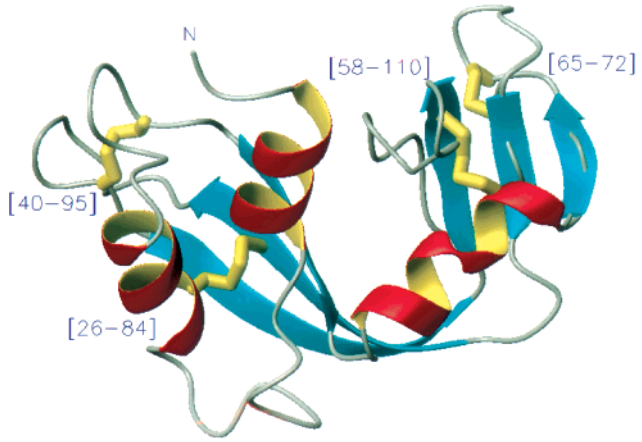

FIGURE 1: High-resolution X-ray structure of wild-type bovine pancreatic ribonuclease A (RNase A), showing its four disulfide bonds (*9*). The 26−84 and 58−110 disulfide bonds are fully buried in the core of the protein, and join well-defined secondary structures (an α-helix and *β*-sheet in both cases). By contrast, the 65−72 and 40−95 disulfide bonds occur near the surface of the protein in turn regions; the 40−95 disulfide bond region exhibits particularly high *B*-factors (*9*, *11*), indicating flexibility in this region. The [C40A,C95A] mutant has a nearly identical structure [as determined by NMR (*10*) and X-ray (*11*) studies], with even more disorder in the 40−95 disulfide bond region (*11*).

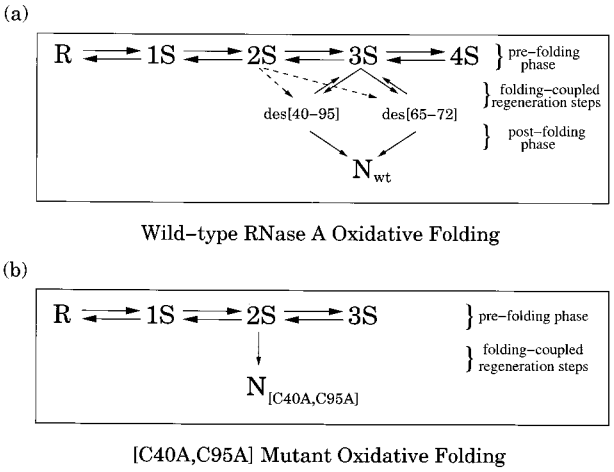

FIGURE 2: Kinetic models of the oxidative folding of (a) wild-type RNase A and (b) the [C40A,C95A] mutant (*6*, *19*). R and 1S−4S are composed of unstructured disulfide species, whereas the three-disulfide species des[40−95] and des[65−72] are folded species with secondary and tertiary structure similar to those of the four-disulfide native species of wild-type RNase A (N_{wt}) (*10*, *21*). The three-disulfide native form of the [C40A,C95A] mutant ($N_{[C40A,C95A]}$) is also well-structured, being analogous to des[40−95]. In the wild-type protein, the major rate-determining step is a reshuffling step from the unstructured 3S ensemble to the two structured des species, while that of the mutant is an oxidation from the unstructured 2S ensemble. Reshuffling is generally rapid in the unstructured *n*S ensembles, but cannot occur in the 3S ensemble of the mutant protein and in the 4S ensemble of wild-type RNase A (scrambled RNase A), since no free thiolate groups are present.

ates these disulfide bonds from the fully reduced state under oxidizing conditions (*15*). In the early *pre-folding* stage of oxidative folding, unstructured disulfide intermediates are populated by redox and reshuffling reactions and reach a steady-state distribution (*6*, *16*−*20*). These intermediates may be grouped into disulfide ensembles labeled by their number of disulfide bonds, e.g., the 1S, 2S, and 3S ensembles (Figure 2). These disulfide ensembles are useful because, under typical oxidative folding conditions (e.g., 25 °C, pH 8.0, and 100 mM oxidized dithiothreitol), the disulfide species interconvert rapidly *within* each such ensemble by thiol−disulfide exchange reactions, whereas the redox reactions between disulfide ensembles are relatively slow. Hence, each disulfide ensemble can be considered as being in thermodynamic equilibrium so that the ratios of disulfide species within the ensemble should reflect their relative free energies (*6*). Therefore, the distribution of disulfide species would provide a clear assessment of the relative free energies involved in forming each pairing of cysteines (*6*). Unfortunately, present analytical methods are not sufficiently developed to measure this distribution of disulfide *species* directly; instead, we can measure the distribution of disulfide *bonds* within each ensemble (as described in Materials and Methods) (*7*, *8*). For the 1S ensemble, the distribution of disulfide bonds is the same as that of the disulfide species, and in special cases (such as the fully oxidized 3S ensemble of the [C40A,C95A] mutant), the distribution of disulfide species can be determined from the distribution of disulfide bonds. It should be noted that fully oxidized ensembles such as the 4S ensemble of wild-type RNase A ("scrambled RNase A") may not represent an equilibrium distribution, since such species have no free thiol groups and, hence, cannot interconvert by disulfide reshuffling.

In the subsequent *post-folding* stage of oxidative folding (*6*, *19*, *20*), structured intermediates such as des[40−95] and des[65−72] are formed (Figure 2; *10*, *21*). The stable tertiary structure of these intermediates protects their buried disulfide bonds from further disulfide-bond reactions, thus causing these species to accumulate well beyond the levels typical of the unstructured ensembles (*6*). According to our present model (*6*, *19*), the formation of such structured disulfide species from unstructured precursors represents the rate-determining process in the oxidative folding under typical regeneration conditions (e.g., 25 °C, pH 8.0, and 100 mM DTT^{ox}). In wild-type RNase A, the major rate-determining steps correspond to the formation of des[65−72] and des-[40−95] by reshuffling from unstructured 3S precursors (*6*, *18*). By contrast, the rate-determining step in the regeneration of the [C40A,C95A] mutant is the oxidation of unstructured 2S precursors to the fully folded three-disulfide native protein (*22*). The coupling of conformational folding and disulfide-bond reactions in these rate-determining steps has been considered recently (*20*).

We report here the relative disulfide-bond populations in the 1S, 2S, and 3S ensembles of the [C40A,C95A] mutant (columns 3, 5, and 7 of Table 1) under near-physiological conditions (25 °C and pH 8). Thirteen of the fifteen possible disulfide bonds are observed; specifically, the 26−65 and 65−84 disulfide bonds are absent from the 1S, 2S, and 3S ensembles of [C40A,C95A] and from the 1S and 2S ensembles of wild-type RNase A. The broad distribution of disulfide bonds in [C40A,C95A] is consistent with our earlier studies (*7*, *8*) and with the rapid reshuffling and lack of stable tertiary structure in these ensembles (*6*). Although recent observations by another group (*23*−*26*) contradict this broad distribution, rigorous cross-checks (described in the Results) show unambiguously that our data are self-consistent whereas the contradictory data are not. The distributions of disulfide bonds in the 1S ensembles of wild-type RNase A and of [C40A,C95A] show a power-law dependence on loop length,

Table 1: Experimental Percentages[a] of Each Disulfide Bond in the 1S, 2S, and 3S Ensembles of [C40A,C95A][b]

disulfide bond	WT 1S	1S		2S		3S	
	exptl	exptl	Δ*S* only	exptl	Δ*S* only	exptl	Δ*S* only
26−58	3.7	5.1	2.7	17.0	9.7	40.0	27.2
26−65	ND	ND	2.0	ND	4.7	ND	10.3
26−72	ND	4.3	1.6	7.0	5.7	8.4	17.0
26−84	1.9	3.5	1.1	11.0	6.5	6.3	8.0
26−110	1.4	2.0	0.6	9.1	4.5	40.9	37.5
58−65	13.5	11.7	26.3	15.8	39.7	22.5	39.5
58−72	9.5	8.5	9.3	9.1	11.9	5.0	13.1
58−84	3.5	4.7	3.7	19.1	13.6	40.6	15.0
58−110	2.2	4.3	1.3	11.3	6.1	3.1	5.2
65−72	56.9	46.8	26.3	71.9	29.4	83.1	30.2
65−84	ND	ND	5.9	ND	9.6	ND	10.5
65−110	0.9	0.3	1.6	2.5	4.7	6.0	9.4
72−84	3.2	5.8	11.7	8.3	29.8	7.4	29.1
72−110	2.9	1.7	2.1	5.5	6.6	5.0	10.5
84−110	0.4	1.3	3.7	12.4	17.6	31.7	37.4

[a] The percentages for the 1S, 2S, and 3S ensembles are normalized to 100, 200, and 300%, respectively. This normalization is chosen so that the disulfide-bond percentage corresponds to a percentage of the disulfide species with that disulfide bond. For example, the 58−65 disulfide bond is found in 15.8% of the protein molecules in the 2S ensemble, although it comprises 7.9% (15.8/2) of the disulfide bonds present. The expression ND indicates that the disulfide bond was not detected, although such species might be present below the detection limit (roughly 0.2%). Boldface type indicates the three native disulfide bonds. [b] The WT 1S column represents the experimentally determined disulfide-bond populations in the 1S ensemble of wild-type RNase A (*7*), normalized so that the sum of percentages in this column equals 100%; i.e., disulfide bonds involving Cys40 or Cys95 in the wild-type 1S ensemble are not counted. However, the 2S wild-type distribution is not included, since it cannot be reasonably compared with the [C40A,C95A] 2S distribution, since the two additional cysteines in the wild-type protein skew the relative distribution of the disulfide bonds. The exptl columns represent the experimental percentages for the 1S, 2S, and 3S ensembles of [C40A,C95A], while the Δ*S* only columns represent the predicted distribution if the unstructured species had the conformational propensities of an ideal freely jointed polymer. The fully oxidized 3S ensemble need not have an equilibrated disulfide-bond distribution, since the 3S species have no free thiol groups for reshuffling reactions. Native [C40A,C95A] is *not* included in the 3S ensemble, which comprises the unstructured intermediates with three disulfide bonds (cf. Figures 2 and 4).

with an exponent that is significantly smaller than the corresponding exponents for either ideal or excluded-volume polymers (*27*−*29*). Significant deviations from this power-law dependence are observed for a few disulfide bonds (Table 1 and Figure 3); in particular, an extraordinary preference for the 65−72 disulfide bond is observed, consistent with earlier disulfide-distribution (*7*, *8*) and peptide studies (*27*−*29*). Under our conditions, this preference does not appear to result from the burial of the cysteines in tertiary structure or from anomalous pK_a values of the cysteines (*30*−*32*), but rather from conformational bias in the backbone. In general, the other disulfide bonds exhibit relatively small deviations from the power-law dependence.

MATERIALS AND METHODS

Materials. The expression, purification, refolding, and characterization of the [C40A,C95A] mutant have been described previously (*7*, *22*). DTT^{ox} (Sigma Chemical Co.) was purified as described by Creighton (*33*). DTT^{red} of the highest purity was purchased from Roche Molecular Biochemicals, and used without further purification. AEMTS

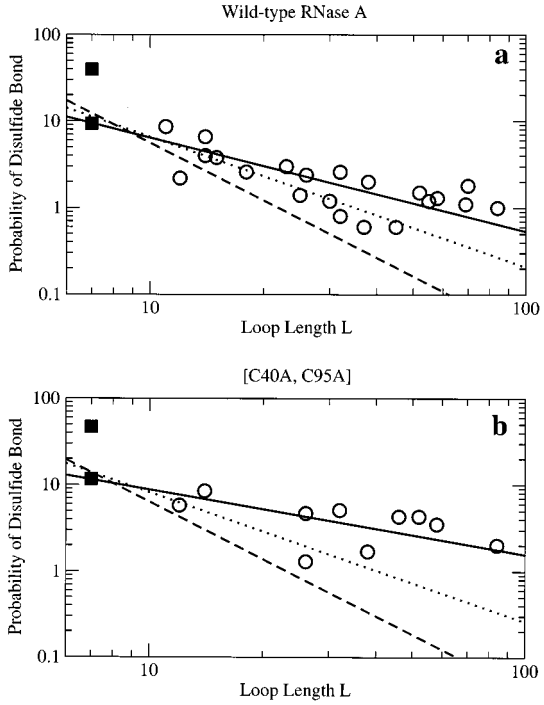

FIGURE 3: (a) Plot of the wild-type 1S disulfide-bond percentages (*7*) vs loop length. The solid line represents the best fit to a power law with an arbitrary exponent ($C = -1.08$), whereas the dotted and dashed lines represent fits to the power laws for ideal chains (*27*) ($C = -1.5$) and for polymers with excluded volume (*28*, *29*) ($C = -2.2$). The experimental percentages for the 58−65 and 65−72 disulfide bonds are indicated by squares, where the 65−72 disulfide bond point is much higher than the 58−65 disulfide bond point (roughly 40 and 10%, respectively). (b) Analogous plot for the 1S disulfide-bond percentages for the [C40A,C95A] mutant (Table 1).

was prepared by the method of Bruice and Kenyon (*34*). NTSB was prepared by the method of Thannhauser et al. (*35*). Trypsin (type III, from bovine pancreas) and α-chymotrypsin (type II, from bovine pancreas) were obtained from Sigma Chemical Co., and used without further purification. All other reagents were of the highest grade commercially available.

Reduction and Regeneration of [C40A,C95A]. [C40A,-C95A] was fully reduced as described previously (*22*). The mutant protein was regenerated from its reduced form at a concentration of 15 μM in a solution of DTT^{ox} (initial concentration of 150 mM), Tris buffer (100 mM, pH 8.0), and 2 mM EDTA. The solution was sparged with argon prior to the addition of DTT^{ox} or protein. Regeneration was allowed to proceed at 25 °C under an atmosphere of argon for 3 h, at which time AEMTS (in a 20−100-fold molar excess) was added to quench the regeneration process rapidly. The blocking process was allowed to proceed at room temperature for 5−10 min, after which the pH was lowered to a value between 4 and 5 with acetic acid. The mixture was then either frozen at −70 °C or injected immediately onto an HPLC column for isolation of the intermediates.

Isolation of Different Disulfide Ensembles. The quenched regeneration mixture prepared above was injected onto an analytical cation-exchange HPLC column [Rainin Hydropore-5-SCX (4.6 mm × 50 mm)]. The HPLC system, buffer composition, and gradient used for isolating different groups of disulfide intermediates are the same as in previous kinetic

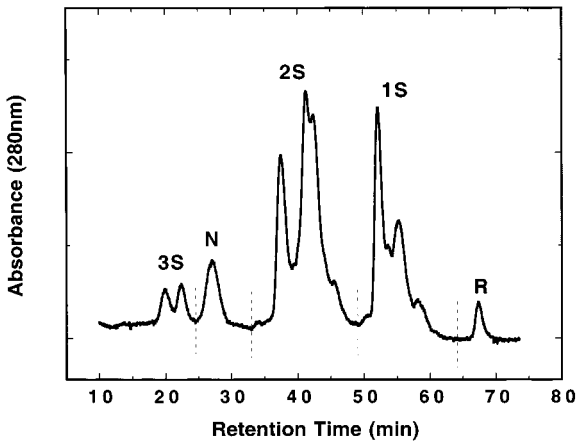

FIGURE 4: Cation-exchange chromatogram for the regeneration of [C40A,C95A]. The regeneration conditions were as follows: 15 μM protein, 150 nm DTT^{ox}, 100 mM Tris buffer, and 2 mM EDTA at pH 8.0 and 25 °C for 3 h. R, 1S, 2S, and 3S represent the AEMTS-blocked reduced and one-, two-, and three-disulfide *intermediate* ensembles, respectively. N represents the regenerated mutant [C40A,C95A]. The vertical dashed lines indicate how each disulfide ensemble was collected in the isolation step. The two 3S peaks are composed predominantly of the disulfide species (26−110,58−84,65−72) (the left peak, eluting at roughly 21 min) and (26−58,65−72,84−110) (the right peak, i.e., the closest peak to N, eluting at roughly 24 min).

experiments (*22*). The different disulfide ensembles are well-resolved, as shown in the typical cation-exchange chromatogram in Figure 4. The fractions corresponding to individual disulfide ensembles (1S, 2S, and 3S) were pooled, as indicated by the vertical dashed lines shown in Figure 4, and dialyzed against three 4 L quantities of 100 mM acetic acid at 4 °C over a period of 36 h. The dialyzed protein solutions were then divided into several fractions and stored at −70 °C.

Proteolytic Digestion. Enzymatic digestion of the isolated AEMTS-blocked R, 1S, 2S, and 3S species was carried out as described previously (*7*, *8*). Briefly, the proteins were digested with trypsin for 1 h, and then by chymotrypsin for an additional 1 h. The pH of the solution was then lowered to 2 with 20% (v/v) TFA. The digested mixtures were stored at −70 °C.

Peptide Mapping. The digests were analyzed by reversed-phase HPLC using a Hewlett-Packard series 1100 system with a binary pump and diode array detector. Absorbance was monitored continuously at 215 nm. A YMC minibore column (ODS AQ 120A S3, 2 mm × 150 mm) was used to separate the tryptic−chymotryptic peptides under the following HPLC conditions. First, an isocratic gradient with 94% buffer A (100% H_2O with 0.05% TFA) and 6% buffer B (50% acetonitrile and 50% H_2O with 0.05% TFA) was run for 10 min; then, the gradient was changed to 65% buffer B (35% buffer A) over a period of 100 min. The flow rate was 0.2 mL/min. With this gradient, most digestion fragments could be resolved on the HPLC chromatogram.

All peptide fragments from the digestion of each disulfide ensemble were collected and lyophilized separately to prepare them for MALDI-TOF mass analysis with a Finniganmat (Lasermat model 2000) mass spectrometer. Samples were prepared by dissolving the lyophilized fragments collected above in 5 μL of 0.05% TFA. This solution (1 μL) was mixed with 1 μL of the matrix (70% acetonitrile and 30% H_2O with 10 mg/mL α-cyano-4-hydroxycinnamic acid) and placed in the mass spectrometer. The errors in the masses determined with this instrument are less than 0.1%.

Disulfide-Bond Analysis. The amount of material in each reversed-phase HPLC peak from the enzymatic digests that contained a disulfide bond was determined quantitatively. A modified disulfide-detection system (DDS), based on the original one developed by Thannhauser et al. (*36*), was connected in series with the UV detector of the HPLC system. This system consisted of the DDS solution [0.5 M Na_2SO_3, 2 mM EDTA, 0.5 mM NTSB, and 200 mM glycine (pH 9.5)] pumped at 0.5 mL/min (isocratic) to a mixing tee, which mixed this solution with the effluent from the UV detector of the HPLC system. The mixed solution then proceeded through a 30 s reaction loop (0.01 in. inside diameter, 20 ft long Teflon tubing) (replacing the reaction coils in the original DDS) to an ISCO UA type 9 detector with a wavelength filter at 410 nm. The signal from the DDS detector is proportional to the number of moles of disulfide bonds eluting at a given time. Therefore, the number of blocked cysteine residues or disulfide bonds in the peptides can be obtained from the integrated disulfide-bond signals.

Reduction and Reblocking. In addition to a mass spectral analysis of each lyophilized peak from the digestion map of each disulfide intermediate, a reduction and reblocking process was also carried out for each disulfide-bond-containing fraction from the digestion map. This is necessary to determine the quantitative composition of each peak in the map, because most of the peaks contain several fragments each. The reduction and reblocking method also serves to confirm the mass spectral analysis. The procedures for reducing and reblocking were the same as those described in previous publications (*7*, *8*).

A further validation of the experimental method was implemented from the determination of the fraction of disulfide-bonded fragments due to peptide−peptide disulfide bonds (as opposed to peptide−AEMTS-blocked disulfide bonds) in the total disulfide signals. Since there are one disulfide and four blocked cysteines in each 1S intermediate of the mutant, the peptide−peptide disulfide bonds should make up one-fifth of the DDS signal. The expected numbers for the 2S and 3S intermediate should be 2/4 and 3/3, respectively. The experimental values agreed with these numbers to within 5% in each experiment.

Normalization of the Relative Disulfide-Bond Percentages. The relative percentage P_b of disulfide bond b is defined here as the sum of the relative percentages P_σ of the disulfide species σ having that disulfide bond. As a consequence of this definition, the relative disulfide-bond percentages of the 1S, 2S, and 3S ensembles sum up to 100, 200, and 300%, respectively (Table 1). The advantage of this normalization is that the relative disulfide-bond percentage P_b reflects the relative percentage of molecules in the ensemble having that disulfide bond. For example, if 100% of the molecules in the 3S ensemble have the 65−72 disulfide bond, then its relative percentage likewise equals 100%. By contrast, if the relative disulfide-bond percentages of the 3S ensemble were normalized to 100% instead of 300%, the relative percentage of 65−72 would be 33%, since 65−72 makes up only one-third of the disulfide bonds present (since every 3S molecule would have two other disulfide bonds in addition to the 65−72 disulfide).

Table 2: Best-Fitting Distribution of the 3S Species in [C40A,C95A][a]

3S disulfide species	est %	SS bond	est SS %	exptl SS %	ΔSS %
(26−58,65−72,84−110)	35.0	26−58	37.8	40.0	−2.2
(26−58,65−84,72−110)	0.1	26−65	0.0	ND	0.0
(26−58,65−110,72−84)	2.7	26−72	7.0	8.4	−1.4
(26−65,58−72,84−110)	0.0	**26−84**	10.5	6.3	4.2
(26−65,58−84,72−110)	0.0	26−110	44.7	40.9	3.8
(26−65,58−110,72−84)	0.0	58−65	16.1	22.5	−6.4
(26−72,58−65,84−110)	3.6	58−72	0.6	5.0	−4.4
(26−72,58−84,65−110)	3.1	58−84	41.3	40.6	0.7
(26−72,58−110,65−84)	0.2	**58−110**	4.2	3.1	1.1
(26−84,58−65,72−110)	6.2	**65−72**	77.2	83.1	−5.9
(26−84,58−72,65−110)	0.3	65−84	0.5	ND	0.5
(26−84,58−110,65−72)	4.0	65−110	6.2	6.0	0.2
(26−110,58−65,72−84)	6.3	72−84	9.0	7.4	1.6
(26−110,58−72,65−84)	0.3	72−110	6.3	5.0	1.3
(26−110,58−84,65−72)	38.2	84−110	38.6	31.7	6.9

rms deviation $\chi^2 = {}^1/_{15}\Sigma(\Delta SS\%)^2 = 3.5$

[a] The estimated percentages for the 3S disulfide *species* (in column 2) are normalized to 100%, whereas the percentages for the 3S disulfide *bonds* (in columns 4 and 5) are normalized to 300%, as explained in the text and in Table 1. The estimated disulfide-bond percentages in column 4 are calculated by adding the percentages of the disulfide species (in column 2) having that disulfide bond. For example, the percentage for the 65−72 disulfide bond (77.2%) is obtained by adding the percentages of the three disulfide species with that disulfide bond (35.0% + 4.0% + 38.2%). Column 6 gives the difference between these estimated disulfide-bond percentages and the experimental percentages; the rms deviation is 3.5%. The disulfide-species percentages in column 2 were obtained by minimizing this rms deviation with respect to the disulfide-species percentages (see Materials and Methods). The native disulfide species and disulfide bonds are indicated by boldface type. The small percentage of the native disulfide species is consistent with the overlapping peaks (and hence, imperfect fractionation) of the structured native species and the unstructured disulfide species of the 3S ensemble.

The percentages in Tables 1 and 2 are reported only for the unstructured disulfide ensembles 1S−3S, collected as described above and in the legend of Figure 4. In particular, the native peak (Figure 4) was *excluded* from this analysis, since we are concerned only with the relative populations of unstructured disulfide species. The native and 3S peaks overlap slightly (Figure 4), however, which may account for the small estimated amount of native [C40A,C95A] reported in Table 2.

Estimation of the 3S Disulfide Species Percentages. The populations of the 15 possible disulfide species of the 3S ensemble were estimated by a Monte Carlo optimization procedure as follows. At each step, a trial distribution of 3S disulfide species is proposed by slightly perturbing the last accepted distribution. The corresponding distribution of disulfide bonds is then calculated as described in Table 2. The agreement of this latter distribution with the experimental disulfide-bond distribution was then assessed by the sum χ^2 of squared deviations. The proposed step was then accepted if the χ^2 for the proposed distribution was lower than that of the previous accepted distribution. Fifty runs of 100 million Monte Carlo steps each were made beginning from random distributions; the lowest χ^2 solution is reported in Table 2. An identical optimization was carried out for a χ^2 defined as the sum of squared *relative* differences from experimental data (data not shown); the final distribution differed insignificantly (generally <0.5%) from the distribution reported in column 2 of Table 2.

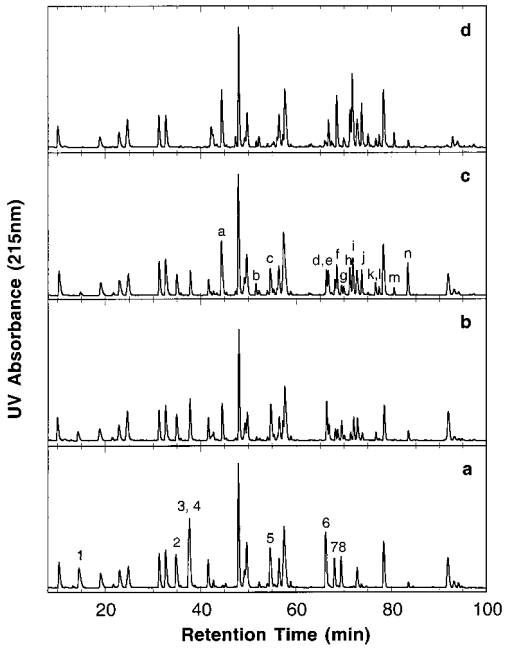

FIGURE 5: Reversed-phase HPLC chromatogram of the tryptic−chymotryptic digestion for various disulfide ensembles of [C40A,C95A]. Panels a−d display the peptide maps for AEMTS-blocked fully reduced and one-, two-, and three-disulfide intermediates, respectively. Numeric labels in panel a denote fragments that contain AEMTS-blocked cysteines. Their assignments (positions in the protein sequence) are as follows: 1, 62−66 (Cys65); 2, 26−31 (Cys26); 3, 67−73 (Cys72); 4, 80−85 (Cys84); 5, 105−115 (Cys110); 6, 47−61 (Cys58); 7, 105−110 (Cys110); and 8, 47−58 (Cys58). Letters in panel c denote fragments that contain peptide−peptide disulfide bonds. Their cysteine pairing assignments are as follows: a, (65, 72); b, (26, 84); c, (26, 72) and (72, 84); d, (72, 84); e, (58, 65); f, (26, 58); g, (65, 110); h, (58, 84); i, (26, 110) and (58, 72); j, (84, 110); k, (72, 110); l, (58, 84); m, (84, 110); and n, (58, 110).

RESULTS

Relative Populations of the Disulfide Bonds in the 1S−3S Ensembles. Figure 5 shows HPLC chromatograms for the tryptic−chymotryptic digests of the AEMTS-blocked R, 1S, 2S, and 3S disulfide species. (The peaks are identified in the legend of Figure 5.) Only 13 of the 15 possible disulfide bonds were identified in the digests of the 1S, 2S, and 3S ensembles; in particular, the 26−65 and 65−84 disulfide bonds were not observed in any digest. The corresponding DDS chromatograms for digests of the AEMTS-blocked R, 1S, 2S, and 3S species are shown in Figure 6. The relative populations of each disulfide bond in the 1S−3S ensembles can be obtained by integrating the peak areas for each disulfide-containing fragment. For peaks that are overlapped or poorly resolved, the relative populations were obtained by combining the DDS data with the information obtained from the reducing and reblocking technique for that peak, as described in Materials and Methods. The relative populations of the disulfide bonds in the 1S−3S ensembles of the [C40A,C95A] mutant are summarized in Table 1.

The 1S disulfide-bond populations for the [C40A,C95A] mutant generally agree with those of wild-type RNase A (Table 1 and Figure 7); the mean magnitude of deviation is 1.4%, if the exceptional case of the 65−72 disulfide is excluded (Table 1). The relative ranks of the wild-type and mutant 1S populations agree closely, with a Spearman rank-

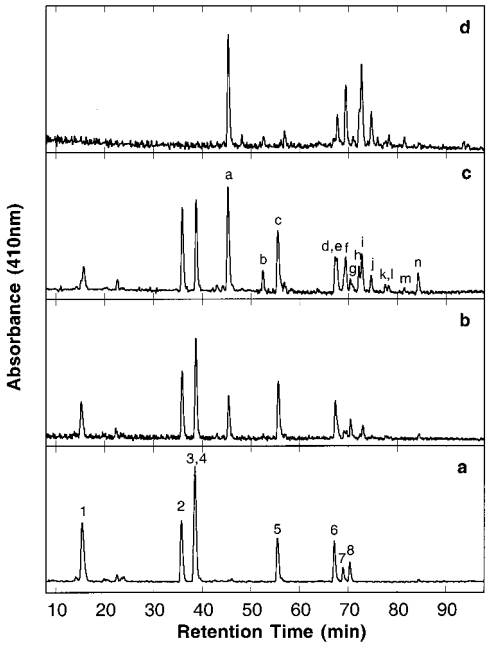

FIGURE 6: Chromatograms for tryptic−chymotryptic digestion of various disulfide ensembles of [C40A,C95A] detected by DDS. Panels a−d display the peptide map for AEMTS-blocked fully reduced and one-, two-, and three-disulfide intermediates, respectively. Labels in panels a and c are the same as in Figure 5.

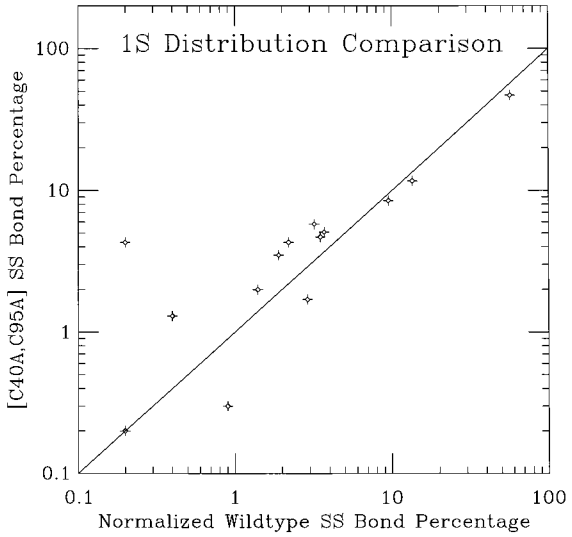

FIGURE 7: Comparison of the disulfide-bond percentages in the 1S ensemble of [C40A,C95A] (Table 1) with those of the corresponding disulfide bonds in the 1S ensemble of wild-type RNase A (*7*), plotted on a log−log scale. The wild-type percentages have been normalized to 100% for comparison purposes; i.e., the measured wild-type percentages have been divided by the sum of the percentages of all disulfide bonds that do not involve Cys40 or Cys95. Disulfide bonds that were not detected are assigned the percentage 0.2%, which may be considered the detection limit of the method. In general, the wild-type and [C40A,C95A] percentages are nearly equal (solid line), indicating that the double mutation has not altered the disulfide bond propensities significantly in the 1S ensemble. This supports the contention that [C40A,C95A] is a reliable model system for studying the oxidative folding of RNase A.

order correlation coefficient of 0.88, corresponding to a Student's *t* score of 6.6 ($q = 8.9 \times 10^{-6}$). This suggests that the distribution of conformations in the corresponding disulfide ensembles has not been altered significantly by the double mutation of Cys40 and Cys95 to alanine. Other data supporting this conclusion are the nearly identical folded conformations adopted by both proteins (*9*−*11*) and the similar average rate constants for disulfide reshuffling among unstructured disulfide species in [C40A,C95A] and the wild-type protein (*22*). The insensitivity of the conformational ensemble to these side-chain mutations is structurally plausible, given that the 40−95 disulfide bond is exposed to solvent in the wild-type protein and occurs in a relatively flexible segment, judging from the local *B*-factors in the X-ray structure (*9*). However, the populations of some disulfide bonds do *not* agree in the wild-type and mutant distributions; most notably, the 26−72 disulfide bond is reasonably well populated in the mutant (4.3%), whereas it is not detected at all in the wild-type population.

Comparison with Other Studies. Our results indicate that nearly all possible disulfide bonds are formed in the DTT regeneration of the [C40A,C95A] mutant (Table 1), which has also been observed in earlier measurements of the disulfide-bond distribution in the 1S and 2S ensembles of wild-type RNase A (*7*, *8*). This broad sampling of the disulfide bonds in the quasi-equilibrium *n*S ensembles of RNase A is consistent with several studies indicating that these ensembles are unstructured and interconvert rapidly (typically on a time scale of 1−2 s at 25 °C and pH 8.0) by thiol−disulfide exchange (*6*).

These findings disagree with the observations of Ruoppolo and co-workers (*23*−*26*). In their experiments, wild-type RNase A is regenerated at pH 7.5 in the presence of a glutathione redox couple and blocked with iodoacetate; the resulting 1S ensemble is then isolated, digested, and analyzed by mass spectrometry. The distribution obtained in this way differs significantly from the distribution measured in our laboratory. Significantly fewer disulfide species were observed [e.g., 12 in their 1S experiments (*25*) vs 24 in our 1S experiments (*7*)], and their distribution seemed to be biased toward short (nearest-neighbor) loops, toward native disulfide bonds, and toward disulfides involving C-terminal cysteines 95 and 110 (*25*).

The data presented in Table 1 may be cross-checked as follows. [C40A,C95A] has six cysteine residues and, hence, has 15 possible disulfide bonds (Table 1). [C40A,C95A] also has 15 3S disulfide *species*, i.e., 15 distinct pairings of the six cysteines to form three disulfide bonds (Table 2). Hence, a unique distribution of the 15 3S disulfide *species* may be determined from the measured distribution of the 3S disulfide *bonds* in the 3S ensemble, by determining the set of 15 disulfide-species percentages that best reproduces the measured disulfide-bond percentages, subject to the constraint that the disulfide-species percentages must be nonnegative. This best-fitting distribution of 3S disulfide species was determined by computational minimization of χ^2 (see Materials and Methods) and is presented in Table 2. A comparison of the predicted 3S disulfide-bond percentages with the experimental 3S disulfide-bond percentages shows an rms error of 3.5%. This analysis predicts that the 3S ensemble is dominated by two species, (26−58,65−72,84−110) and (26−110,58−84,65−72), in roughly equal proportions (Table 2). Hypothesizing that these two species correspond to the two peaks evident in the chromatogram (Figure 4), we carried out peptide mapping on the two 3S peaks separately (data not shown). This analysis confirmed that the peak closer to

the native peak (eluting at roughly 24 min) is predominately (26−58,65−72,84−110), whereas the peak farther from the native peak (eluting at roughly 21 min) is predominately (26−110,58−84,65−72). These independent cross-checks seem to validate our data.

We may apply the same cross-check of attempting to reconstruct the underlying disulfide-species concentrations to the data of Ruoppolo and co-workers, who measured the scrambled 4S disulfide-bond distribution of wild-type RNase A produced in 8 M urea (*23*). Only 12 of the 28 possible disulfide bonds were detected: 26−110, 40−58, 40−84, 40−95, 40−110, 58−84, 58−110, 65−72, 65−110, 84−95, 84−110, and 95−110. However, only two 4S disulfide species can be composed of these disulfide bonds, namely, (26−110,40−95,58−84,65−72) and (26−110,40−58,65−72,84−95), since cysteine 26 can be coupled only with cysteine 110. This result raises the following questions. (1) Which disulfide species gave rise to the remaining six detected disulfide bonds (40−84, 40−110, 58−110, 65−110, 84−110, and 95−110), and (2) why were their other disulfide bonds not detected? The minimal set of disulfide species that contains the 12 *detected* disulfide bonds also contains three *undetected* disulfide bonds, e.g., 26−72, 26−84, and 26−95. Hence, the analytical methods of Ruoppolo and co-workers do not seem to detect all the disulfide bonds that are present in a disulfide ensemble.

Another cross-check involves the relative concentrations of the disulfide-bonded cysteines, which may be obtained by summing the relative concentrations of the disulfide bonds involving a particular cysteine. In a fully oxidized ensemble such as the 3S ensemble of [C40A,C95A] or the 4S ensemble of wild-type RNase A, these summed percentages should equal 100% for all cysteines, since every cysteine is disulfide-bonded in every disulfide species. For example, using the estimated distribution in column 4 of Table 2, the percentage of disulfide-bonded cysteine 58 (which is the sum of the percentages of the 26−58, 58−65, 58−72, 58−84, and 58−110 disulfide bonds) equals 100% exactly, which is true for the relative concentrations of the other five cysteines (Table 2). When this cross-check is applied to our experimental data in column 7 of Table 1, the summed percentage of the six cysteines equals 100 ± 12% (Table 1). However, the data of Ruoppolo and co-workers indicate that the eight cysteines of wild-type RNase A do not have equal net concentrations in the scrambled 4S ensemble; for example, the net concentration of cysteine 110 seems much greater than that of cysteine 26 (*23*). These two cross-checks suggest that the disulfide-bond distribution observed by Ruoppolo and co-workers for scrambled RNase A may be biased. Qualitatively similar biases also appear to be present in their analyses of other disulfide ensembles (*23*−*26*), and are sufficiently great to account for the discrepancies between our data and those of Ruoppolo and co-workers.

It is possible (but unlikely) that the different redox reagents (glutathione in their experiments vs DTT in our experiments) may produce genuinely different disulfide-bond distributions. For example, the distributions could conceivably differ because glutathione can form stable mixed-disulfide species whereas DTT does not. Moreover, DTT is neutral whereas glutathione is charged; hence, the reactivities of these two compounds may differ depending on the local electrostatic environment of each cysteine. However, under both of our solution conditions, disulfide reshuffling within an unstructured disulfide ensemble such as 1S is much more rapid than the redox reactions between ensembles. Hence, it is likely that the distribution of disulfide species within each ensemble is in a quasi-equilibrium that is independent of the redox reactions and, thus, independent of the redox reagent (*6*, *16*, *25*, *37*−*39*). Similarly, it is unlikely that the difference in pH (7.5 in their experiments vs 8.0 in our experiments) would produce significantly different disulfide distributions, given that Ruoppolo and co-workers have observed qualitatively similar distributions at pH 8.0 (*23*) and 7.5 (*24*−*26*). Hence, the discrepancies likely reflect the different analytical methods used by the two groups, as argued above.

The origin of these discrepancies is not obvious. It is possible that unstructured disulfide species were overdigested under the conditions employed by Ruoppolo and co-workers (*23*−*26*). These digestion conditions are sufficiently strong to digest native RNase A and could lead to selective loss of certain disulfide-containing peptides. By contrast, our laboratory uses digestion conditions for unstructured disulfide species (*7*, *8*) that are milder than the digestion conditions applied to structured species such as des[65−72] and the native protein (*18*, *40*, *41*).

DISCUSSION

Dependence of 1S Disulfide-Bond Populations on Loop Length. Under strongly denaturing conditions such as 6 M GdnHCl, the conformational ensemble of RNase A resembles that of a statistical coil (*6*, *42*). Under such conditions, the probability of forming a single disulfide bond b between two residues separated by L residues should vary with the loop length as a power law $P_b \propto L^C$, where C is a constant that depends on the type of polymer. [This formula is equivalent to the well-known polymer loop-entropy formula $\Delta S_b \propto C \ln L$ (*27*).] For ideal freely jointed chains, the exponent C equals −1.5, whereas for polymers with excluded volume interactions, C equals −2.2 for contacts between residues not at the termini of the chain (*29*). [There are slightly different exponents for forming a contact between the two terminal residues and between a terminal residue and an internal residue (*28*, *29*).]

Plotting the wild-type and [C40A,C95A] 1S disulfide-bond percentages versus loop length (Figure 3a,b) shows that these distributions do follow an approximate power law, but that their exponents C are significantly lower than those of either the ideal or excluded-volume polymers, being approximately −1 for the wild-type protein and slightly smaller (≈−3/4) for the [C40A,C95A] mutant. Whether such reduced exponents are peculiar to RNase A or generally representative of denatured proteins (i.e., of unstructured proteins under folding conditions) is a key unanswered question.

As noted by an anonymous referee, it is also possible to divide the wild-type disulfide-bond populations (*7*) into two groups that fit closely to two lines (data not shown). Specifically, the populations of the 40−65, 40−72, 58−65, 58−72, 58−95, 65−72, 65−110, 65−95, and 84−95 disulfide bonds fit closely to a power law of exponent $C \approx -2.5$, while the populations of the 26−40, 26−58, 26−84, 26−95, 26−110, 40−58, 40−95, 40−110, 58−84, 58−110, 72−84, 72−95, 72−110, and 95−110 disulfide bonds fit closely to a power law of exponent $C \approx -0.8$. However,

this grouping does not account for the populations of the undetected disulfide bonds (26−65, 26−72, 40−84, and 65−84) and of the (barely detectable) 84−110 disulfide bond (*7*). The close fit of two power laws to these populations may be simply coincidence, given the uncertainties in the data.

Conformational Propensities Appear To Favor the 65−72 Disulfide Bond. A remarkably strong preference for the 65−72 disulfide bond has been observed in this study (Tables 1 and 2) and in earlier studies of peptides (*30*−*32*) and the 1S and 2S ensembles of wild-type RNase A (*7*, *8*). The population of the 65−72 disulfide bond lies well above the power law that roughly characterizes the other disulfide bonds (Figure 3). A quantitative measure of this preference is the ratio of the 65−72 and 58−65 disulfide-bond populations. Cys58 and Cys72 are both separated by six residues from Cys65; hence, in the absence of enthalpic interactions, the populations of the 58−65 and 65−72 disulfide bonds should be equal (*30*, *31*). However, our results (Tables 1 and 2; *7*, *8*, *31*) show a consistent 4-fold ratio of the populations of the 65−72 and 58−65 disulfide bonds in the 1S ensembles of the wild-type RNase A and the [C40A,C95A] mutant, corresponding to a relative stabilization of 0.8 kcal/mol at room temperature. The 65−72 disulfide bond becomes even more highly populated in the higher disulfide ensembles, being found in 72 and 83% of [C40A,C95A] molecules of the 2S and 3S ensembles, respectively (Tables 1 and 2). As described above in the Results, the two 3S peaks (Figure 4) are composed primarily of two species, (26−110,58−84,65−72) and (26−58,65−72,84−110).

In principle, several factors could account for this preference for the 65−72 disulfide bond. For example, the 65−72 disulfide bond could become buried in local tertiary structure, protecting it from further rearrangement. Alternatively, the 65−72 disulfide bond loop might be stabilized by associating with the 104−124 β-hairpin, which is known to be highly stabilized by hydrophobic interactions. Anomalous pK_a value(s) for one or more cysteine(s) could also contribute to deviations from a power-law distribution.

Experiments on peptide fragments of RNase A, however, clearly show that the preference for the 65−72 disulfide bond does not result from structure in other residues or from accessibility or reactivity factors, but rather from intrinsic conformational biases in the intervening residues (*30*−*32*). The same 4-fold ratio of the 65−72 disulfide bond to the 58−72 disulfide bond has been observed in the fragment of residues 58−72 and several mutants (*31*), while a 6-fold ratio has been measured in a fragment corresponding to residues 50−79 of RNase A (*30*). Therefore, the relative stability of the 65−72 and 58−65 disulfide bonds does not derive from burial of the 65−72 bond or from interactions with residues outside of the segment of residues 58−72. Moreover, pK_a shifts do not seem important, since the preference for the 65−72 disulfide bond is not affected significantly by the K66Q mutation (*31*) and the replacement of the uncharged amide groups at Cys58 and Cys72 in the peptide of residues 50−79 (*30*) with charged terminal amino and carboxylate groups in the peptides of residues 58−72 (*31*). Therefore, we conclude that the preference for the 65−72 disulfide bond arises from short-range conformational biases in the polypeptide backbone. This conclusion is supported by NMR studies of the peptide fragments of residues 61−74 and 65−72 of wild-type RNase A (*32*) that show a clear preference for a type II β-turn at residues 66−69 in these fragments. Such conformational biases favoring (or disfavoring) turns have also been observed in other peptides under physiological conditions (*43*) and in other proteins, e.g., in the rapid formation of the 14−38 disulfide bond of the bovine pancreatic trypsin inhibitor (*44*−*46*).

A few other disulfide bonds deviate significantly from the power-law dependence in that they are not detected (e.g., 26−65, 26−72, 40−84, and 65−84) or are barely detected (e.g., 84−110). At present, we do not have a compelling explanation for these systematic absences. By contrast, the relative percentages of the remaining disulfide bonds do not deviate significantly from the power-law distribution. Hence, we cannot say with certainty whether conformational bias is also present in the distribution of these species, although such biases would be relatively weak compared to those of the 65−72 disulfide bond and those reported by Ruoppolo and co-workers (*23*−*26*). These results are consistent with other experimental observations that the species of the *n*S ensembles are unstructured but are somewhat condensed and possess a weak conformational bias toward the native structure (*6*, *42*).

CONCLUSIONS

We measured the relative disulfide-bond populations of the 1S, 2S, and 3S ensembles of the [C40A,C95A] mutant of RNase A (Table 1). Rigorous cross-checks (described in the Results) indicate that our measurements are consistent, which is not true for the contradictory observations made by another group (*23*−*26*). The disulfide-bond populations exhibit a rough power-law dependence on loop length, but the exponent is significantly lower than those of either ideal or excluded-volume polymers. This is consistent with other structural data (*6*, *42*) indicating that reductively unfolded proteins under folding conditions are condensed relative to such proteins under unfolding conditions such as 6 M GdnHCl. The relative fraction of the 65−72 disulfide bond deviates significantly from this power-law dependence; peptide studies suggest that these deviations result from conformational biases in the backbone, rather than from differing accessibilities or reactivities of the two cysteines. In general, the other disulfide bonds exhibit relatively small deviations from the power-law dependence.

ACKNOWLEDGMENT

We thank M. J. Volles for experimental assistance and H.-C. Shin for reviewing an early draft of the manuscript.

NOTE ADDED AFTER ASAP POSTING

This article was released ASAP on 1/9/02 before final corrections were made. Data was modified in the second and third paragraphs of the Discussion section. The correct version was posted 1/29/02.

REFERENCES

1. Brockwell, D. J., Smith, D. A., and Radford, S. E. (2000) *Curr. Opin. Struct. Biol. 10*, 16−25.
2. Roder, H., and Colon, W. (1997) *Curr. Opin. Struct. Biol. 7*, 15−28.

3. Capaldi, A. P., Shastry, M. C. R., Kleanthous, C., Roder, H., and Radford, S. E. (2001) *Nat. Struct. Biol. 8*, 68−72.
4. Houry, W. A., Rothwarf, D. M., and Scheraga, H. A. (1996) *Biochemistry 35*, 10125−10133.
5. Qi, P. X., Sosnick, T. R., and Englander, S. W. (1998) *Nat. Struct. Biol. 5*, 882−884.
6. Wedemeyer, W. J., Welker, E., Narayan, M., and Scheraga, H. A. (2000) *Biochemistry 39*, 4207−4216.
7. Xu, X., Rothwarf, D. M., and Scheraga, H. A. (1996) *Biochemistry 35*, 6406−6417.
8. Volles, M. J., Xu, X., and Scheraga, H. A. (1999) *Biochemistry 38*, 7284−7293.
9. Wlodawer, A., Svensson, L. A., Sjölin, L., and Gilliland, G. L. (1988) *Biochemistry 27*, 2705−2717.
10. Laity, J. H., Lester, C. C., Shimotakahara, S., Zimmerman, D. E., Montelione, G. T., and Scheraga, H. A. (1997) *Biochemistry 36*, 12683−12699.
11. Pearson, M. A., Karplus, P. A., Dodge, R. W., Laity, J. H., and Scheraga, H. A. (1998) *Protein Sci. 7*, 1255−1258.
12. Neira, J. L., and Rico, M. (1997) *Folding Des. 2*, R1−R11.
13. Raines, R. T. (1998) *Chem. Rev. 98*, 1045−1065.
14. Scheraga, H. A., Wedemeyer, W. J., and Welker, E. (2001) *Methods Enzymol. 341*, 189−221.
15. Anfinsen, C. B., and Haber, E. (1961) *J. Biol. Chem. 236*, 1361−1363.
16. Scheraga, H. A., Konishi, Y., and Ooi, T. (1984) *Adv. Biophys. 18*, 21−41.
17. Rothwarf, D. M., and Scheraga, H. A. (1993) *Biochemistry 32*, 2671−2679.
18. Rothwarf, D. M., Li, Y.-J., and Scheraga, H. A. (1998) *Biochemistry 37*, 3760−3766.
19. Narayan, M., Welker, E., Wedemeyer, W. J., and Scheraga, H. A. (2000) *Acc. Chem. Res. 33*, 805−812.
20. Welker, E., Wedemeyer, W. J., Narayan, M., and Scheraga, H. A. (2001) *Biochemistry 40*, 9059−9064.
21. Shimotakahara, S., Rios, C. B., Laity, J. H., Zimmerman, D. E., Scheraga, H. A., and Montelione, G. T. (1997) *Biochemistry 36*, 6915−6929.
22. Xu, X., and Scheraga, H. A. (1998) *Biochemistry 37*, 7561−7571.
23. Ruoppolo, M., Torella, C., Kanda, F., Panico, M., Pucci, P., Marino, G., and Morris, H. R. (1996) *Folding Des. 1*, 381−390.
24. Ruoppolo, M., Vinci, F., Klink, T. A., Raines, R. T., and Marino, G. (2000) *Biochemistry 39*, 12033−12042.
25. Vinci, F., Ruoppolo, M., Pucci, P., Freedman, R. B., and Marino, G. (2000) *Protein Sci. 9*, 525−535.
26. Orrú, S., Vitagliano, L., Esposito, L., Mazzarella, L., Marino, G., and Ruoppolo, M. (2000) *Protein Sci. 9*, 2577−2582.
27. Poland, D. C., and Scheraga, H. A. (1965) *Biopolymers 3*, 379−399.
28. des Cloizeau, J. (1974) *Phys. Rev. A 10*, 1665−1669.
29. Redner, S. (1980) *J. Phys. A 13*, 3525−3541.
30. Milburn, P. J., and Scheraga, H. A. (1988) *J. Protein Chem. 7*, 377−398.
31. Altmann, K. H., and Scheraga, H. A. (1990) *J. Am. Chem. Soc. 112*, 4926−4931.
32. Talluri, S., Falcomer, C. M., and Scheraga, H. A. (1993) *J. Am. Chem. Soc. 115*, 3041−3047.
33. Creighton, T. E. (1977) *J. Mol. Biol. 113*, 329−341.
34. Bruice, T. W., and Kenyon, G. L. (1985) *Bioorg. Chem. 13*, 77−87.
35. Thannhauser, T. W., Konishi, Y., and Scheraga, H. A. (1984) *Anal. Biochem. 138*, 181−188.
36. Thannhauser, T. W., McWherter, C. A., and Scheraga, H. A. (1985) *Anal. Biochem. 149*, 322−330.
37. Konishi, Y., and Scheraga, H. A. (1980) *Biochemistry 19*, 1308−1316.
38. Konishi, Y., and Scheraga, H. A. (1980) *Biochemistry 19*, 1316−1322.
39. Scheraga, H. A., Konishi, Y., Rothwarf, D. M., and Mui, P. W. (1987) *Proc. Natl. Acad. Sci. U.S.A. 84*, 5740−5744.
40. Li, Y.-J., Rothwarf, D. M., and Scheraga, H. A. (1995) *Nat. Struct. Biol. 2*, 489−494.
41. Welker, E., Narayan, M., Volles, M. J., and Scheraga, H. A. (1999) *FEBS Lett. 460*, 477−479.
42. Navon, A., Ittah, V., Landsman, P., Scheraga, H. A., and Haas, E. (2001) *Biochemistry 40*, 105−118.
43. Montelione, G. T., and Scheraga, H. A. (1989) *Acc. Chem. Res. 22*, 70−76.
44. Dadlez, M., and Kim, P. S. (1996) *Biochemistry 35*, 16153−16164.
45. Dadlez, M. (1997) *Biochemistry 36*, 2788−2797.
46. Zdanowski, K., and Dadlez, M. (1999) *J. Mol. Biol. 287*, 433−445.

BI011893Q